Optimizing DER Participation in Inertial and Primary-frequency Response

Swaroop S. Guggilam, *Student Member, IEEE*, Changhong Zhao, *Member, IEEE*, Emiliano Dall'Anese, *Member, IEEE*, Yu Christine Chen, *Member, IEEE*, and Sairaj V. Dhople, *Member, IEEE*

***Abstract*—This paper develops an approach to enable the optimal participation of distributed energy resources (DERs) in inertial and primary-frequency response alongside conventional synchronous generators. Leveraging a reduced-order model description of frequency dynamics, DERs' synthetic inertias and droop coefficients are designed to meet time-domain performance objectives of frequency overshoot and steady-state regulation. Furthermore, an optimization-based method centered around classical economic dispatch is developed to ensure that DERs share the power injections for inertial- and primary-frequency response in proportion to their power ratings. Simulations for a modified New England test-case system composed of ten synchronous generators and six instances of the IEEE 37-node test feeder with frequency-responsive DERs validate the design strategy.**

***Index Terms*—Distributed energy resources, droop control, model reduction, inertial response, primary frequency response, synthetic inertia.**

I. Introduction

ENSURING power quality in the face of the rapid and admittedly ad-hoc integration of distributed energy resources (DERs) is a challenging task. It is therefore accepted that DERs ought to provide a wide array of ancillary services such as reactive-power support, voltage control, frequency control, and operating reserves to ensure their synergistic operation alongside conventional generators, and seamless integration into the bulk power system [1]–[3]. This paper focuses on frequency control and outlines an approach to optimize the participation of DERs in inertial and primary-frequency response. Particularly, DER synthetic-inertia and droop coefficients are determined such that: i) a collection of DERs and synchronous generators in a given balancing area meet time-domain specifications on frequency overshoot and steady-state frequency regulation, and ii) the DERs inject power in proportion to their power ratings as they partake in inertial and primary-frequency response.

To illustrate the developed approach, consider Fig. 1(a) and Fig. 1(b). The power system in Fig. 1(a) is composed of two conventional synchronous generators and two DERs. The trace in Fig. 1(b) sketches frequency deviation from synchronous frequency, $\omega_{\rm s}$, following a large-signal increase in load, $\Delta P_{\rm load}$. The system frequency reaches a minimum, $\Delta\omega_{\rm nadir}$, at time $t_{\rm nadir}$, and as the generators and DERs respond, it settles to yield the steady-state offset $\Delta\omega_{\rm ss}$. With this general setting in mind, we dwell on the following questions: i) *How does one pick the synthetic inertias and droop slopes of individual DERs to guarantee a prescribed overshoot and steady-state frequency?* ii) *How does one ensure fairness of participation in terms of power provisioning among the DERs?* The answers to these questions hinge on uncovering the mapping between the time-domain specifications $\Delta\omega_{\rm nadir}$ and $\Delta\omega_{\rm ss}$ to the synthetic inertias and droop slopes, $M_{\mathcal{D},1}, M_{\mathcal{D},2}$ and $D_{\mathcal{D},1}, D_{\mathcal{D},2}$—a difficult proposition indeed, given the nonlinear system dynamics involved. This challenge is addressed through the following three steps:

(A) Formulate a reduced second-order model with system frequency and aggregated governor dynamics as states, and load disturbance as input.
(B) Obtain the time-domain frequency trajectory in closed form leveraging the analytical convenience of the second-order model. The trajectory is parameterized by the *effective* damping and inertia, defined to be the sum of generator *and* DER damping and inertia terms.
(C) Disaggregate the effective inertia and damping into individual DER contributions leveraging an optimization-based perspective that ensures DERs respond in proportion to their power ratings.

With regard to the model-reduction step (A), the time constant that captures the dynamics of the aggregated governor is obtained by minimizing the Frobenius norm of the difference of the system matrices corresponding to the original and reduced-order models. Then a closed-form expression is derived for this time constant. Interestingly, one can note that it is not a function of the effective inertia and damping terms which implies that the model-reduction task can be decoupled from the design tasks in (B) and (C). Furthermore, step (C) not only yields the optimal synthetic inertias and droop slopes for the DERs, but also suggests cost functions to dispatch the DERs alongside conventional generators. This addresses the widely appreciated problem of obtaining meaningful cost functions to

S. S. Guggilam and S. V. Dhople are with the Department of Electrical and Computer Engineering, University of Minnesota, Minneapolis, MN, USA. E-mail: {guggi022, sdhople}@umn.edu. C. Zhao and E. Dall'Anese are with the National Renewable Energy Laboratory, Golden, CO, USA. E-mail: {changhong.zhao, emiliano.dallanese}@nrel.gov. Y. C. Chen is with the Department of Electrical and Computer Engineering, The University of British Columbia, Vancouver, British Columbia, Canada. E-mail: chen@ece.ubc.ca.

This work was supported by the U.S. Department of Energy under Contract No. DE-AC36-08GO28308 with the National Renewable Energy Laboratory. The efforts of E. Dall'Anese, S. Guggilam, and S. V. Dhople were supported by the Advanced Research Projects Agency-Energy (ARPA-E) under the Network Optimized Distributed Energy Systems (NODES) program.

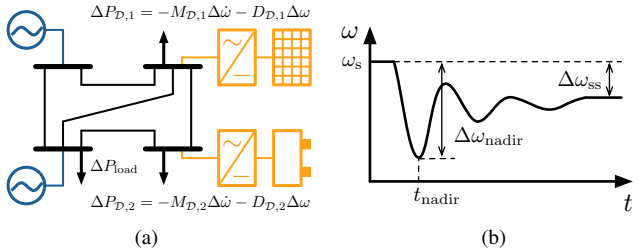

Fig. 1. The design strategy allows one to pick DER synthetic-inertia and droop constants, $M_{\mathcal{D},1}, M_{\mathcal{D},2}$ and $D_{\mathcal{D},1}, D_{\mathcal{D},2}$, (see (a)) to meet specifications pertaining to frequency nadir, $\Delta\omega_{\text{nadir}}$, and steady-state frequency offset, $\Delta\omega_{\text{ss}}$ (see (b)) following a disturbance ΔP_{load}. Furthermore, the synthetic inertias and droop slopes are engineered such that DER power injections $\Delta P_{\mathcal{D},1}, \Delta P_{\mathcal{D},2}$ are proportional to their power ratings through the transient.

dispatch DERs such as photovoltaic systems, wind systems, and energy storage systems that have no fuel costs [4]. Before proceeding, we remark that it might appear we only consider the case where each DER is a single energy-conversion unit. This is without loss of generality; our approach extends to the setting where a collection of DERs are connected to a bus.

The scope of this work specifically encompasses the two areas of model-reduction techniques and optimization-based design; we focus our review of pertinent literature accordingly. There are numerous other aspects such as monetary considerations [5] and controller design respecting features of PV and wind energy conversion systems [6], [7], that, while important in the broad topic of DER integration, are tangential to the present work. Model-reduction methods for power systems is a widely researched topic. A selective modal analysis technique [8] is adopted in [9] to develop a reduced-order model reflecting the structure of the originating model. Another recent effort of note is [10], where model reduction is performed by systematically eliminating elements of system matrices (instead of removing components from the state vector). Most other approaches in this domain invoke well known numerical techniques such as balanced truncation [11], proper orthogonal decomposition [12] and Krylov-subspace methods [13] and apply them to pertinent dynamical models based on application. An overview of common methods is available in [14]. We also bring to attention the effort in [15] where a second-order model for the system frequency response is derived under the unproven assumption that averaged model parameters serve as good proxies for the reduced-order model, and this model is used for setting load shedding relays to contend with under frequency events. Most of the methods discussed above are primarily numerical in nature. They involve matrix manipulations of varying complexity, and these render the task of relating the parameters of the reduced-order model to those of the original model to be intractable. Our approach, on the other hand, allows one to track back the design parameters obtained in the second-order model to the originating model. This is key ingredient of the presented design process which relies on the second-order system description to obtain the frequency trajectory as a function of the system-wide effective inertia and damping.

Shifting focus to optimization-based design methods for DER integration, the efforts in [16], [17] involve optimization problems for scheduling that include DER damping and inertia terms as optimization variables. However to simplify analysis, these methods adopt (the admittedly simple) model where the mechanical power output of the generator changes linearly with frequency deviation. In this regard, proposed approach is more accurate since we retain a detailed dynamical model for the governor in the analysis. Techniques based on minimizing $\mathcal{H}_1$, $\mathcal{H}_2$, and $\mathcal{H}_\infty$ norms are provided in [18]–[21]. These approaches ultimately optimize objective functions which are merely proxies of time-domain criteria like frequency deviations and overshoot. Optimization-based methods to engineer inertia and damping constants to meet frequency- and time-domain specifications are provided in [22] and [23], respectively. These methods are based on numerically computing the system eigenvalues and their sensitivities. The proposed approach is markedly different since it is analytical in nature and presents limited-to-no computational burden. Tuning of inertia and droop coefficients based on system norms or spectral metrics is considered in [24], [25]; and it is assumed that generator inertia can be controlled or modified, whereas we consider external DER support. We also bring to attention our recent work [26] that examined the optimal design of droop slopes for DERs in distribution networks. The goal therein was to guarantee a prescribed primary-frequency regulation value at the feeder-head while ensuring that DERs are not unfairly penalized for their power rating or location within the distribution feeder. Here, we depart from purely steady-state analysis and consider time-domain specifications at the transmission level while acknowledging generator dynamics. Another related effort—albeit for islanded inverter-based systems—is [27], which connects droop control and economic optimality. While our optimization-based disaggregation strategy also uncovers synergies between economic dispatch and real-time control, we study primary *and* inertial control in *mixed* DER-machine systems.

A preliminary version of this work appears in [28]. Here, it is significantly expanded in several important directions. First, a closed-form solution for the time constant that captures aggregate turbine-governor dynamics in the reduced-order model is presented—a significant contribution over [28] that required a numerical solution approach. Second, compared to [28], we focus on time-domain specifications—such as peak overshoot—that are admittedly more challenging to satisfy given the system dynamical models. Furthermore, the optimization-based disaggregation of effective damping and inertia to those of individual DERs is a unique contribution of this paper, and it ensures that the DERs participate fairly (in proportion to their power ratings) in supporting system frequency.

The remainder of this manuscript is organized as follows. Section II outlines the dynamical models adopted for individual generators and DERs, and Section III develops the reduced second-order model for the entire system. Leveraging this second-order model, the approach to design system-wide effective inertia and damping coefficients is described in Section IV, while the optimization-based method to engineer individual DER control coefficients is presented in Section V. In Section VI, the proposed methodologies via numerical case studies is validated. Concluding remarks and directions for

future work are offered in Section VII.

II. System Dynamical Models

In this section, we describe pertinent dynamical models adopted for the generators, DERs, and the network.

A. Transmission Network Model

Consider a transmission grid with buses collected in the set $\mathcal{N}$. Partition the set $\mathcal{N} = \mathcal{D} \cup \mathcal{G}$, where $\mathcal{G}$ is the set of buses that are connected to conventional turbine-based generators and $\mathcal{D}$ is the set of buses connected to frequency-responsive DERs (or their aggregates). For notational and expositional convenience, assume $\mathcal{D} \cap \mathcal{G} = \emptyset$. (This can be readily relaxed.) Buses electrically connected to bus ℓ are collected in the set $\mathcal{N}_\ell$. Transmission lines are assumed to be lossless.[1]

B. Synchronous-generator Dynamics

The dynamics of angular position, frequency, and mechanical-power input are modeled for the generators in the network [29]. Dynamics of power-system stabilizers are typically neglected for studying phenomena pertinent to primary-frequency and inertial response. Automatic voltage regulator dynamics are ignored and it is assumed that the exciter operates at a stable output; therefore, the machine terminal voltage is assumed to be fixed [30], [31]. With these assumptions, dynamics of the $g \in \mathcal{G}$ generator are:

$$\dot{\theta}_g = \omega_g - \omega_{\rm s}, \tag{1a}$$

$$M_{\mathcal{G},g}\dot{\omega}_g = P^{\rm m}_{\mathcal{G},g} - D_{\mathcal{G},g}(\omega_g - \omega_{\rm s}) + P_{\mathcal{G},g} - \sum_{\ell \in \mathcal{N}_g} P_{g\ell}, \tag{1b}$$

$$\tau_g \dot{P}^{\rm m}_{\mathcal{G},g} = -P^{\rm m}_{\mathcal{G},g} + P^{\rm r}_{\mathcal{G},g} - R_{\mathcal{G},g}(\omega_g - \omega_{\rm s}). \tag{1c}$$

Above, θ_g, ω_g, and $P^{\rm m}_{\mathcal{G},g}$ are the rotor electrical angular position, generator frequency, and turbine mechanical power, respectively, and $\omega_{\rm s}$ is the synchronous frequency. Furthermore, $M_{\mathcal{G},g}$ is the inertia constant, $D_{\mathcal{G},g}$ is the load-damping coefficient, $R_{\mathcal{G},g}$ is the inverse of the frequency-power speed-droop regulation constant,[2] τ_g is the turbine time constant, and $P^{\rm r}_{\mathcal{G},g}$ denotes the reference-power setting computed from economic dispatch. Finally, $P_{\mathcal{G},g}$ is the real-power injection at bus g, and $P_{g\ell}$ is the real-power flow from bus g to ℓ. For notational convenience, we define:

$$P^{\rm m}_{\mathcal{G}} := [P^{\rm m}_{\mathcal{G},1}, \ldots, P^{\rm m}_{\mathcal{G},|\mathcal{G}|}]^{\rm T}, P^{\rm r}_{\mathcal{G}} := [P^{\rm r}_{\mathcal{G},1}, \ldots, P^{\rm r}_{\mathcal{G},|\mathcal{G}|}]^{\rm T},$$
$$R_{\mathcal{G}} := [R_{\mathcal{G},1}, \ldots, R_{\mathcal{G},|\mathcal{G}|}]^{\rm T}, \tau := [\tau_1, \tau_2, \ldots, \tau_{|\mathcal{G}|}]^{\rm T}. \tag{2}$$

[1]Notation: The matrix transpose is denoted by $(\cdot)^{\rm T}$, and trace by ${\rm Tr}(\cdot)$. The cardinality of a set is denoted by $|\cdot|$. A diagonal matrix formed with diagonal entries composed of entries of vector x is denoted by ${\rm diag}(x)$; ${\rm diag}\{x, y\}$ is a diagonal matrix with entries of vectors (or matrices) x and y stacked along the main diagonal. The $N \times 1$ vectors of all ones and zeros are denoted by 1_N and 0_N; and the $N \times N$ identity matrix by I_N.

[2]We abuse notation here slightly. Typically, the frequency-power speed-droop regulation constant—and not the inverse—is denoted by $R_{\mathcal{G},g}$ [29].

C. Frequency-responsive DER Model

Assume the following model for DER $d \in \mathcal{D}$:

$$\dot{\theta}_d = \omega_d - \omega_{\rm s}, \tag{3a}$$

$$M_{\mathcal{D},d}\dot{\omega}_d = -D_{\mathcal{D},d}(\omega_d - \omega_{\rm s}) + P_{\mathcal{D},d} - \sum_{\ell \in \mathcal{N}_d} P_{d\ell}. \tag{3b}$$

The droop coefficient $D_{\mathcal{D},d}$ establishes the frequency response of the DER at bus d, the synthetic-inertia constant $M_{\mathcal{D},d}$ determines the inertial response, $P_{\mathcal{D},d}$ is the real power injected at bus d, and $P_{d\ell}$ is the real power flow from bus d to ℓ. The rated real-power output of DER d is denoted by $\overline{P}_{\mathcal{D},d}$. Typically, three-phase grid-tied inverters have power controllers that accept reference setpoints for active and reactive power, and they include phase-locked loops that sense the grid frequency. (See, e.g., [32], [33] for a typical control architecture.) To implement frequency control, one would modulate these reference setpoints with correction terms for damping and inertial control. Furthermore, internal controller dynamics of DERs are ignored since they are implemented at much faster time scales. Studies focused on faster timescales would require the model in (3) to be augmented with further DER-specific dynamics that would dictate the evolution of pertinent power-related DER states and establish connections with the electrical output power.

Before proceeding, a few clarifying comments about the models presented thus far are offered. Frequency-sensitive loads present at generator buses are modeled with the load-damping constant in (1b). Frequency sensitivity of the DERs is captured with the model (3b). Conventional loads are governed by the same model as (3) with $M_{\mathcal{D},d} = D_{\mathcal{D},d} = 0$. Uncontrollable frequency-sensitive loads on load buses are not modeled to simplify notation; they could be straightforwardly incorporated into (3). As expressed, (3) suggests there is an individual DER at bus d. To model an aggregation of DERs with the same capacity all connected to the same bus (e.g., a large wind energy conversion system where the power flows in the collector system are neglected) we can use (3) with the understanding that the droop slopes and synthetic-inertia coefficients for individual DERs in the aggregation are given by $D_{\mathcal{D},d}/|\mathcal{D}_d|$ and $M_{\mathcal{D},d}/|\mathcal{D}_d|$, respectively, where $\mathcal{D}_d$ is the set of DERs at bus d. For the case when DERs are not all connected to the same bus and power flows are not neglected, linearizations of the power-flow equations can facilitate systematic disaggregation of $D_{\mathcal{D},d}$ and $M_{\mathcal{D},d}$ to units within each feeder [26].

III. Reduced Second-order Model

In this section, we obtain a reduced second-order model to capture the dynamics of system frequency.

A. State-space Model

Assume the system initially operates at the steady-state equilibrium point with $\omega_g = \omega_d = \omega_{\rm s}$, $\forall g \in \mathcal{G}, d \in \mathcal{D}$. Defining $\Delta\omega := \omega_g - \omega_{\rm s} = \omega_d - \omega_{\rm s}$, we get from (1b) and (3b)

$$M_{\mathcal{G},g}\Delta\dot{\omega} = P^{\rm m}_{\mathcal{G},g} - D_{\mathcal{G},g}\Delta\omega + P_{\mathcal{G},g} - \sum_{\ell \in \mathcal{N}_g} P_{g\ell} \tag{4}$$

$$M_{\mathcal{D},d}\Delta\dot{\omega} = -D_{\mathcal{D},d}\Delta\omega + P_{\mathcal{D},d} - \sum_{\ell\in\mathcal{N}_d} P_{d\ell}. \tag{5}$$

Using the same $\Delta\omega$ for all nodes is valid for networks where electrical distances are negligible and all the buses have the same frequency even during transients [31], [34], [35]. Summing (4) over all $g \in \mathcal{G}$, and (5) over all $d \in \mathcal{D}$, while recognizing that $\sum_{g\in\mathcal{G}}\sum_{\ell\in\mathcal{N}_g} P_{g\ell} + \sum_{d\in D}\sum_{\ell\in\mathcal{N}_d} P_{d\ell} = 0$ (since the network is lossless) we get

$$M_{\text{eff}}\Delta\dot{\omega} = \sum_{g\in\mathcal{G}} P^{\text{m}}_{\mathcal{G},g} - D_{\text{net}}\Delta\omega - P_{\text{load}}, \tag{6}$$

where P_{load} is the total electrical load given by

$$P_{\text{load}} := -\sum_{g\in\mathcal{G}} P_{\mathcal{G},g} - \sum_{d\in\mathcal{D}} P_{\mathcal{D},d}, \tag{7}$$

and the *effective inertia constant*, M_{eff}, *net damping constant*, D_{net}, and *effective damping constant*, D_{eff}, are defined as

$$M_{\text{eff}} := \sum_{g\in\mathcal{G}} M_{\mathcal{G},g} + \sum_{d\in\mathcal{D}} M_{\mathcal{D},d}, \tag{8}$$

$$D_{\text{net}} := \sum_{g\in\mathcal{G}} D_{\mathcal{G},g} + \sum_{d\in\mathcal{D}} D_{\mathcal{D},d}, \tag{9}$$

$$D_{\text{eff}} := \sum_{g\in\mathcal{G}} (D_{\mathcal{G},g} + R_{\mathcal{G},g}) + \sum_{d\in\mathcal{D}} D_{\mathcal{D},d}. \tag{10}$$

Furthermore, collecting copies of (1c) $\forall g \in \mathcal{G}$, we can write

$$\text{diag}(\tau)\dot{P}^{\text{m}}_{\mathcal{G}} = -P^{\text{m}}_{\mathcal{G}} + P^{\text{r}}_{\mathcal{G}} - R_{\mathcal{G}}\Delta\omega. \tag{11}$$

Combining (6) and (11), yields the state-space model:

$$\dot{x} = Ax + Bu. \tag{12}$$

The state vector and input, $x, u \in \mathbb{R}^{|\mathcal{G}|+1}$, and system matrices, $A, B \in \mathbb{R}^{(|\mathcal{G}|+1)\times(|\mathcal{G}|+1)}$ are given by

$$x = [\Delta\omega, (P^{\text{m}}_{\mathcal{G}})^{\text{T}}]^{\text{T}}, \quad u = [P_{\text{load}}, (P^{\text{r}}_{\mathcal{G}})^{\text{T}}]^{\text{T}}, \tag{13}$$

$$A = \begin{bmatrix} -D_{\text{net}}M^{-1}_{\text{eff}} & M^{-1}_{\text{eff}}1^{\text{T}}_{|\mathcal{G}|} \\ A_R & A_\tau \end{bmatrix},\ B = \text{diag}\{-M^{-1}_{\text{eff}}, -A_\tau\},$$

where $A_\tau := -\text{diag}(\tau)^{-1}$ and $A_R := A_\tau R_{\mathcal{G}}$.

B. Reduced Second-order Model

Consider the following reduced second-order model to capture the frequency dynamics:

$$\dot{x}_{\text{red}} = A_{\text{red}}x_{\text{red}} + B_{\text{red}}u_{\text{red}}. \tag{14}$$

The state vector and input, $x_{\text{red}}, u_{\text{red}} \in \mathbb{R}^2$, and system matrices, $A_{\text{red}}, B_{\text{red}} \in \mathbb{R}^{2\times 2}$ are given by

$$x_{\text{red}} = [\Delta\omega_{\text{red}}, P^{\text{m}}_{\text{red}}]^{\text{T}}, \quad u_{\text{red}} = [P_{\text{load}}, P^{\text{r}}_{\text{red}}]^{\text{T}}, \tag{15}$$

$$A_{\text{red}} = \begin{bmatrix} -D_{\text{net}}M^{-1}_{\text{eff}} & M^{-1}_{\text{eff}} \\ -R_{\mathcal{G},\text{eff}}\tau^{-1}_{\text{red}} & -\tau^{-1}_{\text{red}} \end{bmatrix},\ B_{\text{red}} = \begin{bmatrix} -M^{-1}_{\text{eff}} & 0 \\ 0 & \tau^{-1}_{\text{red}} \end{bmatrix},$$

where $\tau_{\text{red}} > 0$ is represents the time constant of the aggregated governor in the reduced-order model, and

$$P^{\text{r}}_{\text{red}} = \sum_{g\in\mathcal{G}} P^{\text{r}}_{\mathcal{G},g}, \quad R_{\mathcal{G},\text{eff}} = \sum_{g\in\mathcal{G}} R_{\mathcal{G},g}. \tag{16}$$

The order of the original model in (12) is $|\mathcal{G}|+1$. By contrast, the model in (14) is of order 2. The main point of difference in the two models is with regard to the generator governors. While the original model retains governor dynamics for each generator, the reduced-order model contains an aggregated governor.

When $\tau_g = \tau_\ell, \forall g, \ell \in \mathcal{G}$, it is straightforward to show that with the choice $\tau_{\text{red}} = \tau_g$ and $\Delta\omega(0) = \Delta\omega_{\text{red}}(0)$; $\Delta\omega(t) = \Delta\omega_{\text{red}}(t),\ \forall t \geq 0$. When turbine time constants are not equal, the error between $\Delta\omega_{\text{red}}(t)$ and $\Delta\omega(t)$ can be upperbounded. Consider the system (12) (with a matrix A that is diagonalizable and Hurwitz) and the reduced-order counterpart (14). Furthermore, define the matrix

$$\Gamma := \text{diag}\{1, \tau^{-1}_{\text{red}}\text{diag}(\tau)\}, \tag{17}$$

which, we will find useful to quantify the error incurred in model reduction. Suppose the initial conditions for the two dynamical systems at time $t = 0$ are such that $\Delta\omega_{\text{red}}(0) = \Delta\omega(0)$, and $P^{\text{m}}_{\text{red}}(0) = \sum_{g\in\mathcal{G}} P^{\text{m}}_{\mathcal{G},g}(0)$. There exist $\delta, k, \lambda > 0$, such that if $\|(\Gamma - I_{|\mathcal{G}|+1})A)\|_2 < \delta$, we get $\forall t \geq 0$,

$$|\Delta\omega(t) - \Delta\omega_{\text{red}}(t)| < \delta\frac{k}{\lambda}\sup_{0\leq\bar{t}\leq t}\|x(\bar{t})\|_2 + \|A^{-1}Bu(\bar{t})\|_2. \tag{18}$$

For a detailed proof to the above statement, we refer readers to [28]; a brief sketch follows next. Define the auxiliary $|\mathcal{G}|+1$ dimensional dynamical system

$$\dot{\overline{x}} = \overline{A}\overline{x} + \overline{B}u. \tag{19}$$

The state vector, $\overline{x}$, and system matrices, $\overline{A}, \overline{B}$ are given by

$$\overline{x} = [\Delta\overline{\omega}, (\overline{P}^{\text{m}}_{\mathcal{G}})^{\text{T}}]^{\text{T}}, \quad u = [P_{\text{load}}, (P^{\text{r}}_{\mathcal{G}})^{\text{T}}]^{\text{T}}, \tag{20}$$

$$\overline{A} = \Gamma A = \begin{bmatrix} -D_{\text{net}}M^{-1}_{\text{eff}} & M^{-1}_{\text{eff}}1^{\text{T}}_{|\mathcal{G}|} \\ \overline{A}_R & \overline{A}_\tau \end{bmatrix}, \tag{21}$$

$$\overline{B} = \Gamma B = \text{diag}\{-M^{-1}_{\text{eff}}, -\overline{A}_\tau\},$$

where $\overline{A}_\tau := -\tau^{-1}_{\text{red}}I_{|\mathcal{G}|}$, $\overline{A}_R := \overline{A}_\tau R_{\mathcal{G}}$. Since the initial conditions for the system (19) are chosen to match those of (12), i.e., $\overline{x}(0) = x(0)$, the reduced-order model in (14) can be derived from the one in (19) by setting $P^{\text{m}}_{\text{red}} = \sum_{g\in\mathcal{G}} \overline{P}^{\text{m}}_{\mathcal{G},g}$ and $P^{\text{r}}_{\text{red}} = \sum_{g\in\mathcal{G}} P^{\text{r}}_{\mathcal{G},g}$. Furthermore, with initial conditions $\Delta\omega_{\text{red}}(0) = \Delta\overline{\omega}(0)$ and $P^{\text{m}}_{\mathcal{G},\text{red}}(0) = \sum_{g\in\mathcal{G}} \overline{P}^{\text{m}}_{\mathcal{G},g}(0)$, it follows that $\Delta\omega_{\text{red}}(t) = \Delta\overline{\omega}(t),\ \forall t \geq 0$. Now, consider the dynamics of $\Delta x(t) := \overline{x}(t) - x(t)$, which can be expressed as $\Delta\dot{x} = \Gamma A\Delta x + (\Gamma - I_{|\mathcal{G}|+1})\dot{x}$ with $\Delta x(0) = 0_{|\mathcal{G}|+1}$. Treating $\dot{x}$ as an exogenous input, we get

$$\Delta x(t) = \int_{\bar{t}=0}^{t} \text{e}^{\Gamma A(t-\bar{t})}(\Gamma - I_{|\mathcal{G}|+1})\dot{x}(\bar{t})d\bar{t}. \tag{22}$$

There exist $k, \lambda > 0$ such that we can bound $\|\text{e}^{\Gamma A(t-\bar{t})}\|_2 \leq k\text{e}^{-\lambda(t-\bar{t})},\ \forall\ 0 \leq \bar{t} \leq t$ [36]. Using this fact, we get from (22) that

$$\|\Delta x(t)\|_2 \leq \int_{\bar{t}=0}^{t} k\text{e}^{-\lambda(t-\bar{t})} \cdot \|(\Gamma - I_{|\mathcal{G}|+1})(Ax(\bar{t}) + Bu(\bar{t}))\|_2 d\bar{t}, \tag{23}$$

The bound in (18) follows by recognizing $|\Delta\overline{\omega}(t) - \Delta\omega(t)| = |\Delta\omega_{\text{red}}(t) - \Delta\omega(t)| \leq \|\Delta x(t)\|_2$, and under the constraint $\|(\Gamma - I_{|\mathcal{G}|+1})A)\|_2 < \delta$.

C. Choosing an Appropriate Value for $\tau_{\rm red}$

Given the bound on the error between $\Delta\omega_{\rm red}(t)$ and $\Delta\omega(t)$ is directly proportional to $\|(\Gamma - I_{\|\mathcal{G}\|+1})A\|_2$, evidently, a reasonable choice for $\tau_{\rm red}$ would be the following:

$$\tau_{\rm red} = \arg\min_{\widehat{\tau}\geq 0} \|(\Gamma(\widehat{\tau}) - I_{|\mathcal{G}|+1})A\|_2, \tag{24}$$

where $\Gamma(\widehat{\tau}) := \widehat{\tau}^{-1}{\rm diag}\{\widehat{\tau}, {\rm diag}(\tau)\}$. Notice $\|(\Gamma(\widehat{\tau}) - I_{|\mathcal{G}|+1})A\|_2 = \|(\widetilde{\Gamma}(\widehat{\tau}) - I_{|\mathcal{G}|})\widetilde{A}\|_2$, where $\widetilde{\Gamma}(\widehat{\tau}) := \widehat{\tau}^{-1}{\rm diag}(\tau)$, and $\widetilde{A} := [A_R\ A_\tau]$, with $A_\tau = -{\rm diag}(\tau)^{-1}$ and $A_R = A_\tau R_{\mathcal{G}}$ (12). This is because the first row of the matrix $(\Gamma(\widehat{\tau}) - I_{|\mathcal{G}|+1})A$ has all zero entries. Therefore, instead of (24), we solve

$$\tau_{\rm red} = \arg\min_{\widehat{\tau}\geq 0} \|(\widetilde{\Gamma}(\widehat{\tau}) - I_{|\mathcal{G}|})\widetilde{A}\|_2. \tag{25}$$

For any matrix A, $\|A\|_2 \leq \|A\|_{\rm F}$ [37], which is a fact that is particularly useful when applied to our problem. While (25) does not admit a minimizer in analytical closed form, one can obtain an analytical closed-form solution for

$$\arg\min_{\widehat{\tau}\geq 0} \|(\widetilde{\Gamma}(\widehat{\tau}) - I_{|\mathcal{G}|})\widetilde{A}\|_{\rm F}. \tag{26}$$

The minimizer to (26) is given by

$$\tau_{\rm red} = \frac{{\rm Tr}\big({\rm diag}(\tau)\widetilde{A}\widetilde{A}^{\rm T}{\rm diag}(\tau)\big)}{{\rm Tr}({\rm diag}(\tau)\widetilde{A}\widetilde{A}^{\rm T})}. \tag{27}$$

A detailed derivation is provided in Appendix A. We comment on an important point about the choice of $\tau_{\rm red}$ above. Notice that the matrix $\widetilde{A}$ does not depend on $D_{\rm eff}$ and $M_{\rm eff}$, which implies that the reduced-order model can be obtained before attempting design.

IV. Designing Inertia and Damping Coefficients

In this section, we utilize the second-order model to obtain the transfer function from the net-load disturbance to frequency deviation. The inverse Laplace transform yields the time-domain evolution of frequency following a load step as a function of the effective damping and inertia. We can then determine the damping and inertia to obtain a prescribed steady-state frequency regulation and peak overshoot.

A. Transfer Function from Load to Frequency

The s-domain transfer function from the load, $P_{\rm load}$, to frequency deviation, $\Delta\omega$, is obtained from (14) as[3]

$$\frac{\Delta\omega(s)}{P_{\rm load}(s)} = -\frac{k(s+\zeta)}{s^2 + 2\xi\omega_{\rm n}s + \omega_{\rm n}^2}, \tag{28}$$

where the parameters k, ζ, $\omega_{\rm n}$, and ξ are given by

$$\begin{aligned} k &:= M_{\rm eff}^{-1}, \quad \zeta := \tau_{\rm red}^{-1}, \\ \omega_{\rm n} &:= \sqrt{\frac{D_{\rm eff}}{\tau_{\rm red}M_{\rm eff}}}, \quad \xi := \frac{1}{2}\frac{M_{\rm eff} + \tau_{\rm red}D_{\rm net}}{\sqrt{\tau_{\rm red}M_{\rm eff}D_{\rm eff}}}. \end{aligned} \tag{29}$$

[3]We abuse notation slightly and denote the frequency offset corresponding to the reduced-order model by $\Delta\omega$ and not $\Delta\omega_{\rm red}$.

Consider a step change in the load at time $t = 0$ of $\Delta P_{\rm load}$. Substituting $P_{\rm load}(s) = \Delta P_{\rm load}/s$ in (28), we get

$$\Delta\omega(s) = -\frac{\Delta P_{\rm load}k(s+\zeta)}{s(s^2 + 2\xi\omega_{\rm n}s + \omega_{\rm n}^2)}. \tag{30}$$

Taking the inverse Laplace transform above, assuming the system is underdamped, i.e., $0 < \xi < 1$, we get

$$\begin{aligned} \Delta\omega(t) = \Delta\omega_{\rm ss}\Big(1 - \frac{{\rm e}^{-\xi\omega_{\rm n}t}}{\sqrt{1-\xi^2}}\big(&\sin(\omega_{\rm d}t + \varphi) \\ &- \frac{\omega_{\rm n}}{\zeta}\sin(\omega_{\rm d}t)\big)\Big), \end{aligned} \tag{31}$$

where, the parameters $\omega_{\rm d}$, φ, and $\Delta\omega_{\rm ss}$ are given by

$$\begin{aligned} &\omega_{\rm d} = \omega_{\rm n}\sqrt{1-\zeta^2}, \quad \varphi = \tan^{-1}\left(\zeta^{-1}\sqrt{1-\zeta^2}\right), \\ &\Delta\omega_{\rm ss} = -\frac{\Delta P_{\rm load}}{D_{\rm eff}}. \end{aligned} \tag{32}$$

Note that $\Delta\omega_{\rm ss}$ is the steady-state frequency offset, i.e., $\lim_{t\to\infty}\Delta\omega(t) = \Delta\omega_{\rm ss}$.

B. Steady-state Frequency Regulation

The steady-state frequency-regulation is the ratio of change in real-power net-load to the change in steady-state frequency, and it is typically specified in units of MW/0.1 Hz [38]. Denote the specified value of the frequency regulation by $R_{P/\omega}$. Notice from (32) that the effective damping constant should be picked as

$$D_{\rm eff} = -\frac{\Delta P_{\rm load}}{\Delta\omega_{\rm ss}} = R_{P/\omega}, \tag{33}$$

to ensure this specification is met. With $D_{\rm eff}$ at hand, individual DER damping coefficients should be picked to satisfy (10).

C. Peak Overshoot

The frequency nadir, $\Delta\omega_{\rm nadir}$, is defined as the system frequency at the first time $t_{\rm nadir} > 0$ (following the load disturbance) at which $\frac{d\Delta\omega}{dt}\big|_{t=t_{\rm nadir}} = 0$. The peak overshoot specification is defined as:

$$\omega_{\rm peak}^{\%} = \frac{\Delta\omega_{\rm nadir}}{\Delta\omega_{\rm ss}} \cdot 100, \tag{34}$$

where $\Delta\omega_{\rm ss}$ is the steady-state frequency offset that the system settles to at the post-disturbance equilibrium. (See Fig. 1 for an illustration.) In general, given the generator and DER dynamical models in (1) and (3), it is intractable to relate system parameters to the peak overshoot. However, the second-order reduced model allows us to do so. From (31), we see that $t_{\rm nadir}$ is given by the solution of the following equation:

$$\begin{aligned} &{\rm e}^{-\xi\omega_{\rm n}t_{\rm nadir}}\Big(\omega_{\rm n}\xi\sin(\omega_{\rm d}t_{\rm nadir} + \varphi) - \omega_{\rm d}\cos(\omega_{\rm d}t_{\rm nadir} + \varphi) \\ &+ \zeta^{-1}\omega_{\rm n}^2\xi\sin(\omega_{\rm d}t_{\rm nadir}) - \zeta^{-1}\omega_{\rm n}\omega_{\rm d}\cos(\omega_{\rm d}t_{\rm nadir})\Big) = 0. \end{aligned}$$

Elementary trigonometric manipulations simplify the above to

$$\tan(\omega_{\rm d}t_{\rm nadir}) = \frac{\omega_{\rm d}}{\xi\omega_{\rm n} - \zeta}, \tag{35}$$

from which we obtain $t_{\rm nadir}$ as:

$$t_{\rm nadir} = \omega_{\rm d}^{-1}\tan^{-1}\left(\frac{\omega_{\rm d}}{\xi\omega_{\rm n}-\zeta}\right) \tag{36}$$
$$= 2\rho^{-1}\tau_{\rm red}^{-1}M_{\rm eff}\tan^{-1}\left(\frac{\rho}{M_{\rm eff}+\tau_{\rm red}^{-1}D_{\rm net}-2M_{\rm eff}\tau_{\rm red}^{-2}}\right),$$

where, to contain notation, we define

$$\rho := \sqrt{4\tau_{\rm red}^{-1}M_{\rm eff}D_{\rm eff}-(M_{\rm eff}+\tau_{\rm red}^{-1}D_{\rm net})^2}. \tag{37}$$

The second equality in (36), and (37) follow from (29) and (32). Substituting $t_{\rm nadir}$ from (36) above in (31) we get:

$$\begin{aligned}\Delta\omega_{\rm nadir} &= \Delta\omega(t_{\rm nadir})\\ &= \Delta\omega_{\rm ss}{\rm e}^{-\xi\omega_{\rm n}t_{\rm nadir}}\sqrt{\omega_{\rm n}^2+\zeta^2-2\zeta\xi\omega_{\rm n}}.\end{aligned} \tag{38}$$

The peak overshoot is therefore given by:

$$\begin{aligned}\omega_{\rm peak}^{\%} &= \frac{\Delta\omega_{\rm nadir}}{\Delta\omega_{\rm ss}}\cdot 100\\ &= \sqrt{\frac{R_{\mathcal{G},\rm eff}}{\tau_{\rm red}M_{\rm eff}}}{\rm e}^{\frac{2M_{\rm eff}\tau_{\rm red}^{-2}-M_{\rm eff}-\tau_{\rm red}^{-1}D_{\rm net}}{2M_{\rm eff}\tau_{\rm red}^{-1}}t_{\rm nadir}}\cdot 100,\end{aligned} \tag{39}$$

where the second equality above follows from leveraging the definitions in (29) and (32). With $D_{\rm eff}$ picked to satisfy (33), and given $\omega_{\rm peak}^{\%}$, note that (39) is a nonlinear algebraic equation in $M_{\rm eff}$. Solving for $M_{\rm eff}$ from above, the DER synthetic inertias should be picked to satisfy (8).

The above design strategy only establishes constraints on the sum of DER damping and synthetic-inertia coefficients. There are many (indeed, infinite) possibilities to disaggregate this sum into individual values $D_{\mathcal{D},d}$, $M_{\mathcal{D},d}$. We focus on a choice that is optimal in the sense that it ensures power sharing next. Furthermore, we use the overshoot and frequency regulation as design metrics without loss of generality. Indeed, given (31), one could focus on other specifications, e.g., rate of change of frequency and settling time.

V. Optimization-based Disaggregation

In this section, we present an optimization-based perspective to disaggregate the system-wide effective inertia and damping constants into DER synthetic-inertia and droop slopes such that the DERs share power in proportion to their ratings.

A. Economic Dispatch Problem Incorporating DERs

At the transmission level, the system operator conducts economic dispatch, e.g., every 5-10 minutes, to determine the reference power injections for the generators and DERs to meet the system load. Given the models in (1) and (3), such a problem takes the form:[4]

$$\min_{P^{\rm r}_{\mathcal{G},g},g\in\mathcal{G},P_{\mathcal{D},d},d\in\mathcal{D}} \sum_{g\in\mathcal{G}}c_{\mathcal{G},g}(P^{\rm r}_{\mathcal{G},g})+\sum_{d\in\mathcal{D}}c_{\mathcal{D},d}(P_{\mathcal{D},d}) \tag{40a}$$
$$\text{s.t.}\quad \sum_{g\in\mathcal{G}}P^{\rm r}_{\mathcal{G},g}+\sum_{d\in\mathcal{D}}P_{\mathcal{D},d}+\sum_{g\in\mathcal{G}}P_{\mathcal{G},g}=0 \tag{40b}$$
$$\underline{P}^{\rm r}_{\mathcal{G},g}\le P^{\rm r}_{\mathcal{G},g}\le\overline{P}^{\rm r}_{\mathcal{G},g},\quad \forall g\in\mathcal{G} \tag{40c}$$
$$\underline{P}_{\mathcal{D},d}\le P_{\mathcal{D},d}\le\overline{P}_{\mathcal{D},d},\quad \forall d\in\mathcal{D}. \tag{40d}$$

We assume that the cost functions $c_{\mathcal{G},g}(\cdot)$ and $c_{\mathcal{D},d}(\cdot)$ are strictly convex and twice continuously differentiable. Denote the Lagrange multiplier corresponding to the power-balance equality constraint (40b) by λ. Constraints (40c) and (40d) impose power limits on generators and DERs, respectively. The Karush-Kuhn-Tucker (KKT) conditions [39], and strict convexity of the objective function (40a) imply that (40) has a unique set of optimizers $\{P^\star_{\mathcal{D},d}\}_{d\in\mathcal{D}}$, $\{P^{{\rm r},\star}_{\mathcal{G},g}\}_{g\in\mathcal{G}}$, $\lambda^\star$ which satisfy:

$$c'(P^\star_{\mathcal{D},d}) := \left.\frac{dc_{\mathcal{D},d}}{dP_{\mathcal{D},d}}\right|_{P^\star_{\mathcal{D},d}} = -\lambda^\star,$$
$$\text{if } \underline{P}_{\mathcal{D},d}<P^\star_{\mathcal{D},d}<\overline{P}_{\mathcal{D},d} \tag{41}$$
$$c'(P^\star_{\mathcal{D},d})>-\lambda^\star,\quad \text{if } P^\star_{\mathcal{D},d}=\underline{P}_{\mathcal{D},d} \tag{42}$$
$$c'(P^\star_{\mathcal{D},d})<-\lambda^\star,\quad \text{if } P^\star_{\mathcal{D},d}=\overline{P}_{\mathcal{D},d} \tag{43}$$
$$\sum_{g\in\mathcal{G}}P^{{\rm r},\star}_{\mathcal{G},g}+\sum_{d\in\mathcal{D}}P^\star_{\mathcal{D},d}+\sum_{g\in\mathcal{G}}P_{\mathcal{G},g}=0. \tag{44}$$

The uniqueness of $\lambda^\star$ holds as long as *not* all the optimal $P^{{\rm r},\star}_{\mathcal{G},g}$, $g\in\mathcal{G}$ and $P^\star_{\mathcal{D},d}$, $d\in\mathcal{D}$ reach their limits. Let $\mathcal{D}'$ denote the set of DERs whose optimal economic dispatch decisions do not reach their power limits, i.e.,

$$\mathcal{D}' := \left\{d\in\mathcal{D}\,\middle|\,\underline{P}_{\mathcal{D},d}<P^\star_{\mathcal{D},d}<\overline{P}_{\mathcal{D},d}\right\}.$$

Then a DER $d\in\mathcal{D}\backslash\mathcal{D}'$ cannot respond to both over- and under-frequency events, since its power cannot change further in one direction. We consider the scenario where only bi-directional, symmetric response is allowed, and thus exclude the set $\mathcal{D}\backslash\mathcal{D}'$ of DERs from participating in inertial and primary-frequency response. For notational simplicity, let $\mathcal{D}'=\mathcal{D}$, i.e., assume that none of the DERs reaches its power limit. However, the analysis can be straightforwardly extended to the case where $\mathcal{D}'\subset\mathcal{D}$, by setting $M^\star_{\mathcal{D},d}=D^\star_{\mathcal{D},d}=0$ for $d\in\mathcal{D}\backslash\mathcal{D}'$.

B. Optimizing DER Power Injections

With this problem in place, we now discuss how the DER power injections can be optimized to meet a change in the load across time scales pertaining to inertial- and primary-frequency response. To this end, consider that the real-power load changes by an amount $\Delta P_{\rm load}$ at time $t=0$. To ensure that the DERs respond *optimally*, their real-power injections would have to be the solutions of the following optimization problem which follows directly from (40):

$$\min_{P^{\rm in}_{\mathcal{D},d}(t),d\in\mathcal{D}} \int_{t=0}^{\infty}\sum_{d\in\mathcal{D}}c_{\mathcal{D},d}(P^{\rm in}_{\mathcal{D},d}(t))dt \tag{45}$$
$$\text{s.t.}\quad \sum_{g\in\mathcal{G}}P^{\rm in}_{\mathcal{G},g}(t)+\sum_{d\in\mathcal{D}}P^{\rm in}_{\mathcal{D},d}(t)+\sum_{g\in\mathcal{G}}P_{\mathcal{G},g}-\Delta P_{\rm load}=0,$$

where, we denote $P^{\rm in}_{\mathcal{G},g}(t)$ and $P^{\rm in}_{\mathcal{D},d}(t)$ to be the real power injected by generator g and DER d at time t. Note that unlike (40), the problem in (45) is not intended for dispatch. It is purely intended as a stepping stone to engineer the DER

[4] While the model and notation in (3) applies to DERs *and* conventional loads, *only* the DERs are dispatched. This is slightly at odds with the notation adopted in (40).

droop slopes and synthetic inertias. The cost function in (45) builds off the one in (40a). There are two key points of departure: i) the integral is intended to optimally engineer the DER power injections over a time horizon corresponding to primary-frequency and inertial response, and ii) the terms capturing the cost attributable to conventional generators are dropped since the generator dynamics (1) are fixed (the parameters $D_{\mathcal{G},g}, R_{\mathcal{G},g}, M_{\mathcal{G},g}$ are fixed). The problem in (45) is patently difficult to solve and yields limited insights. This is because it is infinite dimensional and the droop slopes and synthetic inertias of the DERs—the terms we set out to engineer—do not appear as decision variables. Leveraging insights from the generator and DER dynamical models in (1) and (3), we claim that the problem below is a surrogate to (45):

$$\min_{M_{\mathcal{D},d}, D_{\mathcal{D},d}, d\in\mathcal{D}} \int_{t=0}^{\infty} \sum_{d\in\mathcal{D}} \widetilde{c}_{\mathcal{D},d}(M_{\mathcal{D},d}, D_{\mathcal{D},d})dt \tag{46a}$$

$$\text{s.t.} \quad \Big(\sum_{d\in\mathcal{D}} M_{\mathcal{D},d} + \sum_{g\in\mathcal{G}} M_{\mathcal{G},g}\Big)\Delta\dot{\omega}(t) \tag{46b}$$
$$+ \Big(\sum_{d\in\mathcal{D}} D_{\mathcal{D},d} + \sum_{g\in\mathcal{G}} (R_{\mathcal{G},g} + D_{\mathcal{G},g})\Big)\Delta\omega(t) + \Delta P_{\text{load}} = 0.$$

Above, we define the shorthand

$$\widetilde{c}_{\mathcal{D},d} := c_{\mathcal{D},d}(P^{\star}_{\mathcal{D},d} - M_{\mathcal{D},d}\Delta\dot{\omega}(t) - D_{\mathcal{D},d}\Delta\omega(t)), \tag{47}$$

and the constraint (46b) follows from (45) by recognizing:

$$P^{\text{in}}_{\mathcal{D},d}(t) = P^{\star}_{\mathcal{D},d} - D_{\mathcal{D},d}\Delta\omega(t) - M_{\mathcal{D},d}\Delta\dot{\omega}(t),$$
$$P^{\text{in}}_{\mathcal{G},g}(t) \approx P^{\text{r},\star}_{\mathcal{G},g} - (D_{\mathcal{G},g} + R_{\mathcal{G},g})\Delta\omega(t) - M_{\mathcal{G},g}\Delta\dot{\omega}(t).$$

Additionally, as a design requirement, we impose the power-balance constraint

$$\Delta P_{\text{load}} + D_{\text{eff}}\Delta\omega(t) + M_{\text{eff}}\Delta\dot{\omega}(t) = 0, \tag{48}$$

where D_{eff} and M_{eff} are the effective damping and inertia provided by both generators and DERs; see (8) and (10). (Given the generator and DER dynamical models in (1) and (3), we note that (48) is exactly satisfied in the limits $t \to 0$ and $t \to \infty$.) From (44), (48), we can rewrite (46) as:

$$\min_{M_{\mathcal{D},d}, D_{\mathcal{D},d}, d\in\mathcal{D}} \int_{t=0}^{\infty} \sum_{d\in\mathcal{D}} \widetilde{c}_{\mathcal{D},d}(M_{\mathcal{D},d}, D_{\mathcal{D},d})dt \tag{49a}$$

$$\text{s.t.} \quad \Big(M_{\text{eff}} - \sum_{d\in\mathcal{D}} M_{\mathcal{D},d} - \sum_{g\in\mathcal{G}} M_{\mathcal{G},g}\Big)\Delta\dot{\omega}(t) \tag{49b}$$
$$+ \Big(D_{\text{eff}} - \sum_{d\in\mathcal{D}} D_{\mathcal{D},d} - \sum_{g\in\mathcal{G}} (D_{\mathcal{G},g} + R_{\mathcal{G},g})\Big)\Delta\omega(t) = 0.$$

Let us denote the Lagrange multiplier corresponding to the equality constraint (49b) by $\widetilde{\lambda}(t)$. Since the cost function $\widetilde{c}(\cdot)$ is strictly convex, the Euler-Lagrange conditions [40] indicate that the problem (46) has a unique set of optimizers $\{M^{\star}_{\mathcal{D},d}, D^{\star}_{\mathcal{D},d}\}_{d\in\mathcal{D}}$, $\widetilde{\lambda}^{\star}(t)$ which satisfy $\forall t$:

$$\frac{\partial \widetilde{c}_{\mathcal{D},d}}{\partial M_{\mathcal{D},d}}\bigg|_{M^{\star}_{\mathcal{D},d}, D^{\star}_{\mathcal{D},d}, \Delta\dot{\omega}^{\star}(t), \Delta\omega^{\star}(t)} - \widetilde{\lambda}^{\star}(t)\Delta\dot{\omega}^{\star}(t) = 0 \tag{50}$$

$$\frac{\partial \widetilde{c}_{\mathcal{D},d}}{\partial D_{\mathcal{D},d}}\bigg|_{M^{\star}_{\mathcal{D},d}, D^{\star}_{\mathcal{D},d}, \Delta\dot{\omega}^{\star}(t), \Delta\omega^{\star}(t)} - \widetilde{\lambda}^{\star}(t)\Delta\omega^{\star}(t) = 0, \tag{51}$$

$$\Big(M_{\text{eff}} - \sum_{d\in\mathcal{D}} M^{\star}_{\mathcal{D},d} - \sum_{g\in\mathcal{G}} M_{\mathcal{G},g}\Big)\Delta\dot{\omega}^{\star}(t) \tag{52}$$
$$+ \Big(D_{\text{eff}} - \sum_{d\in\mathcal{D}} D^{\star}_{\mathcal{D},d} - \sum_{g\in\mathcal{G}} (D_{\mathcal{G},g} + R_{\mathcal{G},g})\Big)\Delta\omega^{\star}(t) = 0.$$

Above, $\widetilde{\lambda}^{\star}(t)$ is the optimal value of the Lagrange multiplier corresponding to the equality constraint (49b), and $\Delta\omega^{\star}(t)$ and $\Delta\dot{\omega}^{\star}(t)$ are the optimal trajectories of $\Delta\omega(t)$ and $\Delta\dot{\omega}(t)$ (generated with $M^{\star}_{\mathcal{D},d}$ and $D^{\star}_{\mathcal{D},d}$). Recognizing from (47) that

$$\frac{\partial \widetilde{c}_{\mathcal{D},d}}{\partial M_{\mathcal{D},d}} = -c'(P^{\star}_{\mathcal{D},d} - M_{\mathcal{D},d}\Delta\dot{\omega}(t) - D_{\mathcal{D},d}\Delta\omega(t))\Delta\dot{\omega}(t),$$
$$\frac{\partial \widetilde{c}_{\mathcal{D},d}}{\partial D_{\mathcal{D},d}} = -c'(P^{\star}_{\mathcal{D},d} - M_{\mathcal{D},d}\Delta\dot{\omega}(t) - D_{\mathcal{D},d}\Delta\omega(t))\Delta\omega(t),$$

we get from (50) and (51), that

$$c'(P^{\star}_{\mathcal{D},d} - M^{\star}_{\mathcal{D},d}\Delta\dot{\omega}^{\star}(t) - D^{\star}_{\mathcal{D},d}\Delta\omega^{\star}(t)) = -\widetilde{\lambda}^{\star}(t). \tag{53}$$

In other words, the optimal synthetic-inertia and droop slopes should be such that the marginal cost of power provided by the DERs is the same across all DERs. Notice that the above formulation yields a continuous-time marginal price. This has been observed in other applications related to power-systems dispatch, albeit at slower time scales [41], [42].

C. Disaggregating DER Synthetic Inertias and Damping

Considering $-D^{\star}_{\mathcal{D},d}\Delta\omega^{\star}(t) - M_{\mathcal{D},d}\Delta\dot{\omega}^{\star}(t)$ as a small perturbation on $P^{\star}_{\mathcal{D},d}$, we expand $c'(P^{\star}_{\mathcal{D},d} - M^{\star}_{\mathcal{D},d}\Delta\dot{\omega}^{\star}(t) - D^{\star}_{\mathcal{D},d}\Delta\omega^{\star}(t))$ in a first-order Taylor series around $P^{\star}_{\mathcal{D},d}$ as

$$c'(P^{\star}_{\mathcal{D},d} - M^{\star}_{\mathcal{D},d}\Delta\dot{\omega}^{\star}(t) - D^{\star}_{\mathcal{D},d}\Delta\omega^{\star}(t)) \approx c'_{\mathcal{D},d}(P^{\star}_{\mathcal{D},d})$$
$$- c''_{\mathcal{D},d}(P^{\star}_{\mathcal{D},d})M^{\star}_{\mathcal{D},d}\Delta\dot{\omega}^{\star}(t) - c''_{\mathcal{D},d}(P^{\star}_{\mathcal{D},d})D^{\star}_{\mathcal{D},d}\Delta\omega^{\star}(t).$$

Leveraging (41) and (53), and defining $\Delta\lambda(t) := \widetilde{\lambda}^{\star}(t) - \lambda^{\star}$, we can reorganize terms above to get

$$c''_{\mathcal{D},d}(P^{\star}_{\mathcal{D},d})M^{\star}_{\mathcal{D},d}\Delta\dot{\omega}^{\star}(t) + c''_{\mathcal{D},d}(P^{\star}_{\mathcal{D},d})D^{\star}_{\mathcal{D},d}\Delta\omega^{\star}(t) = \Delta\lambda(t).$$

Since the above constraint is true $\forall d \in \mathcal{D}$, we get $\forall d, d' \in \mathcal{D}$

$$(c''_{\mathcal{D},d}(P^{\star}_{\mathcal{D},d})M^{\star}_{\mathcal{D},d} - c''_{\mathcal{D},d'}(P^{\star}_{\mathcal{D},d'})M^{\star}_{\mathcal{D},d'})\Delta\dot{\omega}^{\star}(t)$$
$$+ (c''_{\mathcal{D},d}(P^{\star}_{\mathcal{D},d})D^{\star}_{\mathcal{D},d} - c''_{\mathcal{D},d'}(P^{\star}_{\mathcal{D},d'})D^{\star}_{\mathcal{D},d'})\Delta\omega^{\star}(t) = 0.$$

Since this constraint must hold $\forall d, d' \in \mathcal{D}$ and $\forall t \geq 0$, the optimal synthetic-inertia and droop coefficients satisfy

$$\begin{aligned} c''_{\mathcal{D},d}(P^{\star}_{\mathcal{D},d})M^{\star}_{\mathcal{D},d} &= c''_{\mathcal{D},d'}(P^{\star}_{\mathcal{D},d'})M^{\star}_{\mathcal{D},d'}, \\ c''_{\mathcal{D},d}(P^{\star}_{\mathcal{D},d})D^{\star}_{\mathcal{D},d} &= c''_{\mathcal{D},d'}(P^{\star}_{\mathcal{D},d'})D^{\star}_{\mathcal{D},d'}, \end{aligned} \tag{54}$$

Taken together, (52) and (54) indicate that the optimal synthetic-inertia and droop slopes satisfy:

$$M^{\star}_{\mathcal{D},d} = \frac{M_{\text{eff}} - \sum_{g\in\mathcal{G}} M_{\mathcal{G},g}}{c''_{\mathcal{D},d}(P^{\star}_{\mathcal{D},d}) \sum_{\ell\in\mathcal{D}} 1/c''_{\mathcal{D},\ell}(P^{\star}_{\mathcal{D},\ell})}, \tag{55}$$

$$D^{\star}_{\mathcal{D},d} = \frac{D_{\text{eff}} - \sum_{g\in\mathcal{G}} (D_{\mathcal{G},g} + R_{\mathcal{G},g})}{c''_{\mathcal{D},d}(P^{\star}_{\mathcal{D},d}) \sum_{\ell\in\mathcal{D}} 1/c''_{\mathcal{D},\ell}(P^{\star}_{\mathcal{D},\ell})}. \tag{56}$$

Next, the cost function that guarantees power sharing is derived.

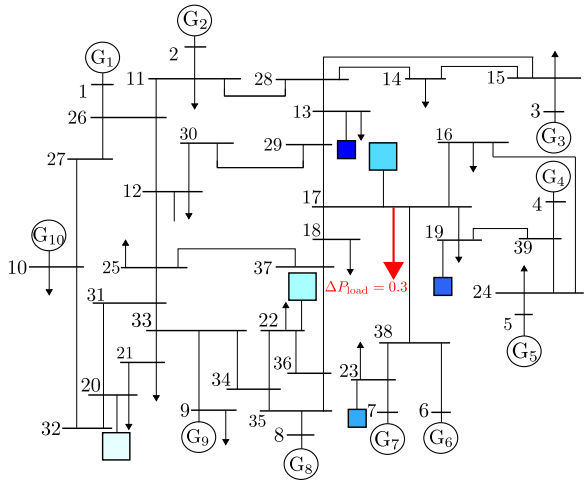

Fig. 2. Modified New England 39-bus system with 10 conventional generators and 6 frequency-responsive DERs (marked as squares). The DERs at buses $20, 22, 17$ have twice the power rating as the ones at buses $23, 19, 13$.

D. Ensuring DER Contributions are Proportional to Ratings

Consider the setting where the excess power provided by the DERs for primary-frequency and inertial response is in proportion to their ratings. In particular,

$$\frac{D^\star_{\mathcal{D},d}\Delta\omega^\star(t) + M^\star_{\mathcal{D},d}\Delta\dot{\omega}^\star(t)}{\overline{P}_{\mathcal{D},d}} = \frac{D^\star_{\mathcal{D},d'}\Delta\omega^\star(t) + M^\star_{\mathcal{D},d'}\Delta\dot{\omega}^\star(t)}{\overline{P}_{\mathcal{D},d'}}, \quad \forall\, d, d' \in \mathcal{D}.$$

Recognizing (54), we see that this translates to requiring $\overline{P}_{\mathcal{D},d}c''_{\mathcal{D},d}(P^\star_{\mathcal{D},d}) = \overline{P}_{\mathcal{D},d'}c''_{\mathcal{D},d'}(P^\star_{\mathcal{D},d'})$, which further implies that the cost functions should be such that $c''_{\mathcal{D},d}(P^\star_{\mathcal{D},d}) = \kappa\overline{P}^{-1}_{\mathcal{D},d}$, where $\kappa > 0$ is some constant. An example of such a cost function is $c_{\mathcal{D},d}(P_{\mathcal{D},d}) = \frac{1}{2}\frac{P^2_{\mathcal{D},d}}{\overline{P}_{\mathcal{D},d}}$, which results in the following droop slopes and synthetic-inertia constants:

$$M^\star_{\mathcal{D},d} = \frac{M_{\text{eff}} - \sum_{g\in\mathcal{G}} M_{\mathcal{G},g}}{\overline{P}^{-1}_{\mathcal{D},d}\sum_{\ell\in\mathcal{D}}\overline{P}_{\mathcal{D},\ell}}, \tag{57a}$$

$$D^\star_{\mathcal{D},d} = \frac{D_{\text{eff}} - \sum_{g\in\mathcal{G}}(D_{\mathcal{G},g} + R_{\mathcal{G},g})}{\overline{P}^{-1}_{\mathcal{D},d}\sum_{\ell\in\mathcal{D}}\overline{P}_{\mathcal{D},\ell}}. \tag{57b}$$

VI. Numerical Simulation Results

We simulate the 10-machine New-England power system, where $\mathcal{N} = \{1, 2, 3, \ldots, 39\}$, with generators connected at buses in $\mathcal{G} = \{1, 2, \ldots, 10\}$ [43], [44], and aggregated DERs modeled at buses $\mathcal{D} = \{13, 17, 19, 20, 22, 23\}$. A schematic is shown in Fig. 2. Although we consider an aggregated DER model for designing the synthetic inertias and droop coefficients, for simulation purposes we consider the IEEE 37-node test feeder shown in Fig. 3 with the actual DERs shown as blue circles. The feeder capacities at buses $20, 22, 17$ have twice the power rating as the ones at buses $23, 19, 13$; i.e., $\overline{P}_{\mathcal{D},20} = \overline{P}_{\mathcal{D},22} = \overline{P}_{\mathcal{D},17} = 2\overline{P}_{\mathcal{D},23} = 2\overline{P}_{\mathcal{D},19} = 2\overline{P}_{\mathcal{D},13}$. Pertinent model parameters and ratings are listed in Appendix B. For convenience, power and impedance values are in per unit [pu] with base 1000 [MVA], unless otherwise specified.

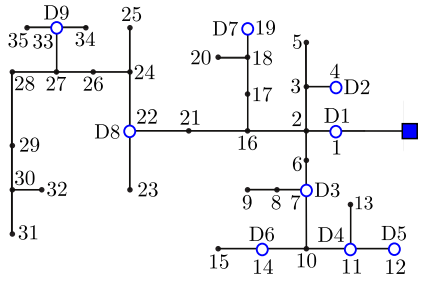

Fig. 3. Modified IEEE 37-node distribution test feeder model. The model includes nine frequency-responsive DERs (blue circles), $\text{D}1, \ldots, \text{D}9$. Five instances of this feeder with similar topology but different ratings are connected to buses $\mathcal{D} = \{13, 17, 19, 20, 22, 23\}$ in the transmission system in Fig. 2 (illustrated as colored squares). The ratings are as follows $\overline{P}_{\mathcal{D},20} = \overline{P}_{\mathcal{D},22} = \overline{P}_{\mathcal{D},17} = 2\overline{P}_{\mathcal{D},23} = 2\overline{P}_{\mathcal{D},19} = 2\overline{P}_{\mathcal{D},13}$.

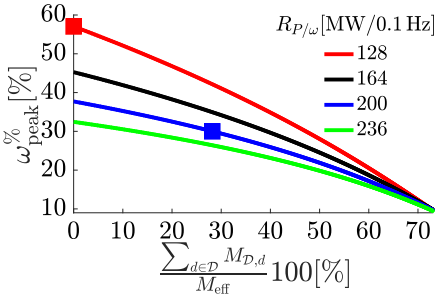

Fig. 4. Frequency overshoot, $\omega^{\%}_{\text{peak}}$, versus the inertia contributed by the DERs for different values of steady-state frequency regulation, $R_{P/\omega}$. The solid-red square corresponds to the case without frequency support from DERs, and the solid-blue square corresponds to the case with DERs. Corresponding time-domain results are in Figs. 5(a), 5(b).

A. Exploring the Design Space

Here, we examine the impact of DER penetration level—quantified in terms of the fraction of total inertia in the system provided by the DERs—on the frequency response of the system, from both steady-state and dynamic perspectives. Figure 4 denotes the peak frequency overshoot, $\omega^{\%}_{\text{peak}}$, as a function of the inertia provided by the DERs (expressed as a fraction of the effective inertia) for different values of the steady-state frequency regulation, $R_{P/\omega}$. The plots are obtained from (33) and (39). When inertial contributions from the DERs are small, the damping has a pronounced impact on the overshoot. When DERs contribute approximately 70% of the total inertia in the system, there are diminishing returns in increasing damping to achieve further reduction in overshoot. The red square represents the case with no DERs (only generators provide frequency response) and it yields a frequency-regulation $R_{P/\omega} = 128[\text{MW}/0.1\text{Hz}]$ and overshoot $\omega^{\%}_{\text{peak}} \approx 57\%$. Now, suppose we wish to improve performance to obtain overshoot $\omega^{\%}_{\text{peak}} = 30\%$ and regulation $R_{P/\omega} = 200[\text{MW}/0.1\text{Hz}]$ (this is marked as the solid-blue square in Fig. 4). This would require DERs to provide (in aggregate) $\sum_{d\in\mathcal{D}} D_{\mathcal{D},d} = 43.07$ and $\sum_{d\in\mathcal{D}} M_{\mathcal{D},d} = 61.44$ (which is approximately 30% of M_{eff}). The individual synthetic inertias and damping coefficients for the DERs are then determined from (57a) and (57b), respectively.

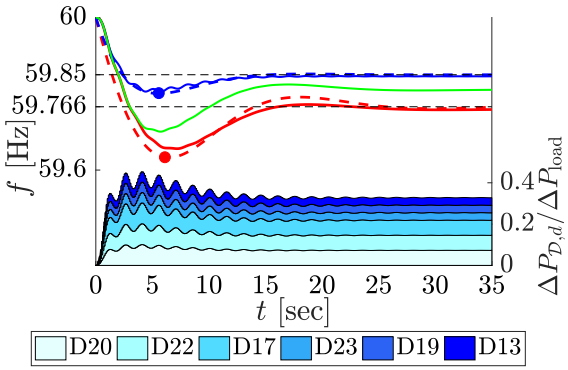

(a)

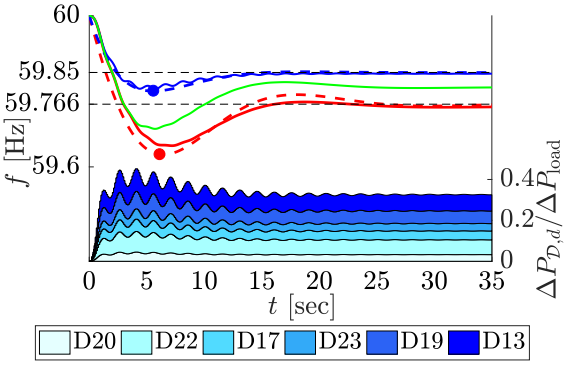

(b)

Fig. 5. [Top panes] (a),(b) Dashed (red and blue) lines are generated by simulating the second-order model, circles represent the analytically predicted frequency nadirs, and solid (red, green, and blue) lines are obtained from the PST simulation, with the green curve corresponding to UFLS. The blue curves correspond to the setting where DER frequency support is engineered to yield steady-state frequency regulation $R_{P/\omega} = 200[\text{MW}/0.1\text{Hz}]$ and overshoot $\omega^{\%}_{\text{peak}} = 30\%$. [Bottom panes] (a) Power outputs of aggregated DERs indicate power sharing in proportion to capacities; (b) power outputs of aggregated DERs are not optimized.

B. Time-domain Simulations

With the DER damping and inertia constants in place, we now present time-domain simulation results to validate the design process. These are performed with the Power System Toolbox (PST) [45]. At time $t = 0$, the load at bus 17 undergoes a step increase of $\Delta P_{\text{load}} = 0.3$. Consider the trajectories in the top pane of Fig. 5(a). Dashed traces correspond to simulations from the reduced-order model, while solid traces correspond to those obtained from PST. Trajectories in red correspond to the case where the DERs do not participate in frequency response (i.e., $D_{\mathcal{D},d} = M_{\mathcal{D},d} = 0, \forall d \in \mathcal{D}$). Compared to this base case, we show the frequency response due to the same load increase with the DER synthetic-inertia and droop-control parameters designed as described in Section VI-A with blue traces. Notice that the frequency support provided by the DERs yields a damped response, a smaller frequency nadir, and a lower steady-state frequency offset. In both cases, we notice that trajectories generated from the second-order model closely match those obtained from the PST simulation. This establishes the accuracy of the reduced-order model and validates the assumptions leading up to it (note that the PST model considers a lossy network, and includes voltage-regulator dynamics and a detailed two-axis machine model). Solid red and blue circles mark the analytically computed frequency-nadir points (from (38)).

The proposed method is also compared to the conventional under frequency load shedding (UFLS) approach. It is assumed that only generators in the transmission network provide primary frequency response and under frequency load shedding (UFLS) capability of $0.05\,[\text{pu}]$ is available when system frequency drops below $59.75\,[\text{Hz}]$ [15]. The corresponding frequency trajectories are shown as green curves in Fig. 5(a) and 5(b). It can be seen that although UFLS yields a damped response and better frequency offset value compared to the case when only generators offer frequency response, the trajectory cannot be engineered to meet performance specifications.

Next, we comment on the power outputs from the 6 feeders with DERs. These are plotted for two cases in the bottom panes of Figs 5(a) and 5(b). Figure 5(a) shows the case where droop slopes and synthetic inertias for the feeders are selected according to the criteria (57a) and (57b). The DER aggregations indeed share the load increase in proportion to their power ratings across time scales pertinent to inertial and primary-frequency response. In Fig 5(b), droop slopes and synthetic inertias are selected randomly, but subject to satisfy the peak overshoot and frequency offset requirements. It is evident that in both figures 5(a) and 5(b) the system frequency response is identical, but the power supplied by each feeder is different. The allocation in 5(b) could be construed to be unfair, given that the capacities of the DERs are such that $\overline{P}_{\mathcal{D},20} = \overline{P}_{\mathcal{D},22} = \overline{P}_{\mathcal{D},17} = 2\overline{P}_{\mathcal{D},23} = 2\overline{P}_{\mathcal{D},19} = 2\overline{P}_{\mathcal{D},13}$.

VII. Concluding Remarks & Future Work

This paper outlined an approach to ensure DERs participate optimally in primary-frequency and inertial response by leveraging a reduced-order model description of frequency dynamics. The proposed method determines DER synthetic inertias and droop coefficients such that a collection of DERs and synchronous generators meet specifications on frequency overshoot and steady-state frequency regulation while ensuring that DER power injections are in proportion to their power ratings. Options for future work include extending the method to multiple balancing areas and settings where the common-frequency assumption does not hold. Extending the optimization setup to account for non-convex cost functions, power flow constraints, thermal limits on lines, reserves for inertial- and primary-frequency response, and distribution-network power flows (following, e.g., the approach in [26]) are other compelling directions for future work.

Appendix

A. Derivation of (27)

Begin with the optimization problem:

$$\min_{\widehat{\tau} \geq 0} \|(\Gamma(\widehat{\tau}) - I_{|\mathcal{G}|+1})A\|_{\text{F}}^2. \tag{58}$$

Using the variable substitution $\chi := 1/\widehat{\tau}$, (58) can be rewritten as $\min_{\chi \geq 0} \|(\overline{\Gamma}(\chi) - I_{|\mathcal{G}|+1})A\|_{\text{F}}^2$, where $\overline{\Gamma}(\chi) =$

$\chi \mathrm{diag}\{\chi^{-1}, \mathrm{diag}(\tau)\}$. Since the first row of matrix $\overline{\Gamma}(\chi) - I_{|\mathcal{G}|+1}$ contains all zeros, it follows that

$$\|(\overline{\Gamma}(\chi) - I_{|\mathcal{G}|+1})A\|_{\mathrm{F}}^2 = \|(\chi \mathrm{diag}(\tau) - I_{|\mathcal{G}|})\widetilde{A}\|_{\mathrm{F}}^2.$$

Next, using

$$\|\chi \mathrm{diag}(\tau)\widetilde{A} - \widetilde{A}\|_{\mathrm{F}}^2 = \mathrm{Tr}((\chi \mathrm{diag}(\tau)\widetilde{A} - \widetilde{A})(\chi \mathrm{diag}(\tau)\widetilde{A} - \widetilde{A})^{\mathrm{T}})$$

problem (58) can be equivalently expressed as:

$$\min_{\chi \geq 0} \ \chi^2 \, \mathrm{Tr}(\mathrm{diag}(\tau)\widetilde{A}\widetilde{A}^{\mathrm{T}}\mathrm{diag}(\tau)) - 2\chi \, \mathrm{Tr}(\mathrm{diag}(\tau)\widetilde{A}\widetilde{A}^{\mathrm{T}}).$$

Applying the first-order optimality condition one can find the optimal $\chi^\star$, and it follows that the minimizer to (26) is:

$$\tau_{\mathrm{red}} = \frac{\mathrm{Tr}\big(\mathrm{diag}(\tau)\widetilde{A}\widetilde{A}^{\mathrm{T}}\mathrm{diag}(\tau)\big)}{\mathrm{Tr}(\mathrm{diag}(\tau)\widetilde{A}\widetilde{A}^{\mathrm{T}})}. \tag{59}$$

B. Parameters for the Case Studies

Synchronous frequency, $\omega_{\mathrm{s}} = 2\pi 60 \, [\mathrm{rad\,sec}^{-1}]$.

Parameters modified from the standard IEEE New-England system: Generator damping coefficients: $D_{\mathcal{G},1} = \cdots = D_{\mathcal{G},10} = 1.5$, droop coefficients: $R_{\mathcal{G},1} = 2.5, R_{\mathcal{G},2} = 5.7, R_{\mathcal{G},3} = 6.5, R_{\mathcal{G},4} = 6.3, R_{\mathcal{G},5} = 5.1, R_{\mathcal{G},6} = 6.5, R_{\mathcal{G},7} = 5.6, R_{\mathcal{G},8} = 5.4, R_{\mathcal{G},9} = 8.3, R_{\mathcal{G},10} = 10$, turbine time constants: $\tau_1 = 4, \tau_2 = 5, \tau_3 = 6, \tau_4 = 4.5, \tau_5 = 5, \tau_6 = 5.5, \tau_7 = 5, \tau_8 = 4.5, \tau_9 = 5, \tau_{10} = 6 \, [\mathrm{sec}]$.

Parameters modified from the standard IEEE 37-node test feeder [46]: Balanced operation is assumed, and data from phase 2 is utilized for the simulation. We add $y_{kk}^{\mathrm{sh}} = 0.004 + \mathrm{i}0.005, \forall \, k \in \{2, \ldots, 18\} \subset \mathcal{B}_3$ and $y_{kk}^{\mathrm{sh}} = 0.006 + \mathrm{i}0.007, \forall \, k \in \{18, \ldots, 35\} \subset \mathcal{B}_3$. The base voltage is $4.8 \, [\mathrm{kV}]$. The base rating for $\overline{P}_{\mathcal{D},13}$ is $50 \ [\mathrm{MW}]$.

REFERENCES

[1] F. Teng, V. Trovato, and G. Strbac, "Stochastic scheduling with inertia-dependent fast frequency response requirements," *IEEE Transactions on Power Systems*, vol. 31, no. 2, pp. 1557–1566, March 2016.

[2] E. Hirst and B. Kirby, *Electric-power ancillary services*. Oak Ridge National Laboratory Oak Ridge, 1996.

[3] Y. G. Rebours, D. S. Kirschen, M. Trotignon, and S. Rossignol, "A survey of frequency and voltage control ancillary services—part I: Technical features," *IEEE Transactions on Power Systems*, vol. 22, no. 1, pp. 350–357, Feb 2007.

[4] J. A. Taylor, S. V. Dhople, and D. S. Callaway, "Power systems without fuel," *Renewable and Sustainable Energy Reviews*, vol. 57, pp. 1322–1336, 2016.

[5] C. Y. Tee and J. B. Cardell, "Market integration of distributed resources through coordinated frequency and price droop," *IEEE Transactions on Smart Grid*, vol. 5, no. 4, pp. 1556–1565, 2014.

[6] J. Seuss, M. J. Reno, M. Lave, R. J. Broderick, and S. Grijalva, "Advanced inverter controls to dispatch distributed PV systems," in *IEEE 43rd Photovoltaic Specialists Conference (PVSC)*, 2016, pp. 1387–1392.

[7] C. Shao, X. Wang, M. Shahidehpour, X. Wang, and B. Wang, "Security-constrained unit commitment with flexible uncertainty set for variable wind power," *IEEE Transactions on Sustainable Energy*, vol. 8, no. 3, pp. 1237–1246, July 2017.

[8] I. J. Pérez-Arriaga, G. C. Verghese, and F. C. Schweppe, "Selective modal analysis with applications to electric power systems, part I: Heuristic introduction," *IEEE transactions on power apparatus and systems*, no. 9, pp. 3117–3125, 1982.

[9] D. Apostolopoulou, P. W. Sauer, and A. D. Domínguez-García, "Balancing authority area model and its application to the design of adaptive agc systems," *IEEE Transactions on Power Systems*, vol. 31, no. 5, pp. 3756–3764, September 2016.

[10] Y. Levron and J. Belikov, "Reduction of power system dynamic models using sparse representations," *IEEE Transactions on Power Systems*, To be published, 2017.

[11] H. Sandberg and A. Rantzer, "Balanced truncation of linear time-varying systems," *IEEE Transactions on Automatic Control*, vol. 49, no. 2, pp. 217–229, Feb 2004.

[12] K. Willcox and J. Peraire, "Balanced model reduction via the proper orthogonal decomposition," *AIAA journal*, vol. 40, no. 11, pp. 2323–2330, 2002.

[13] Z. Zhu, G. Geng, and Q. Jiang, "Power System Dynamic Model Reduction Based on Extended Krylov Subspace Method," *IEEE Transactions on Power Systems*, vol. 31, no. 6, pp. 4483–4494, November 2016.

[14] J. Chow, *Power System Coherency and Model Reduction*, ser. Power Electronics and Power Systems. Springer, New York, 2013.

[15] P. M. Anderson and M. Mirheydar, "An adaptive method for setting underfrequency load shedding relays," *IEEE Transactions on Power Systems*, vol. 7, no. 2, pp. 647–655, May 1992.

[16] H. Chávez, R. Baldick, and S. Sharma, "Governor rate-constrained opf for primary frequency control adequacy," *IEEE Transactions on Power Systems*, vol. 29, no. 3, pp. 1473–1480, May 2014.

[17] F. Teng, M. Aunedi, D. Pudjianto, and G. Strbac, "Benefits of Demand-Side Response in Providing Frequency Response Service in the Future GB Power System," *Frontiers in Energy Research*, vol. 3, p. 36, 2015.

[18] B. K. Poolla, S. Bolognani, and F. Dörfler, "Optimal placement of virtual inertia in power grids," *IEEE Transactions on Automatic Control*, To be published, 2017.

[19] M. Pirani, J. W. Simpson-Porco, and B. Fidan, "System-theoretic performance metrics for low-inertia stability of power networks," *arXiv preprint arXiv:1703.02646*, 2017.

[20] D. Gross, S. Bolognani, B. Poolla, and F. Dörfler, "Increasing the Resilience of Low-inertia Power Systems by Virtual Inertia and Damping," in *IREP Bulk Power System Dynamics & Control Symposium, in press*, 2017.

[21] A. Mešanović, U. Münz, and C. Heyde, "Comparison of H_∞, H_2, and pole optimization for power system oscillation damping with remote renewable generation," *IFAC-PapersOnLine*, vol. 49, no. 27, pp. 103–108, 2016.

[22] T. S. Borsche, T. Liu, and D. J. Hill, "Effects of rotational inertia on power system damping and frequency transients," in *IEEE Conference on Decision and Control*, December 2015, pp. 5940–5946.

[23] T. S. Borsche and F. Dörfler, "On placement of synthetic inertia with explicit time-domain constraints," *arXiv:1705.03244*, 2017.

[24] E. Rakhshani, D. Remon, A. M. Cantarellas, and P. Rodriguez, "Analysis of derivative control based virtual inertia in multi-area high-voltage direct current interconnected power systems," *IET Generation, Transmission & Distribution*, vol. 10, no. 6, pp. 1458–1469, 2016.

[25] S. Chatzivasileiadis, T. L. Vu, and K. Turitsyn, "Remedial actions to enhance stability of low-inertia systems," in *IEEE Power and Energy Society General Meeting (PESGM)*, 2016, pp. 1–5.

[26] S. S. Guggilam, C. Zhao, E. Dall'Anese, Y. C. Chen, and S. V. Dhople, "Optimizing power-frequency droop characteristics of distributed energy resources," *IEEE Transactions on Power Systems*, To be published 2017.

[27] F. Dörfler, J. W. Simpson-Porco, and F. Bullo, "Breaking the Hierarchy: Distributed Control and Economic Optimality in Microgrids," *IEEE Transactions on Control of Network Systems*, vol. 3, no. 3, pp. 241–253, September 2016.

[28] S. S. Guggilam, C. Zhao, E. Dall'Anese, Y. C. Chen, and S. V. Dhople, "Engineering inertial and primary-frequency response for distributed energy resources," in *IEEE Conference on Decision and Control*, 2017, To be published. [Online]. Available: https://arxiv.org/abs/1706.03612

[29] P. Kundur, *Power System Stability and Control*. McGraw-Hill, 1994.

[30] A. D. Domínguez-García, "Models for impact assessment of wind-based power generation on frequency control," in *Control and Optimization Methods for Electric Smart Grids*. Springer, 2012, pp. 149–165.

[31] M. D. Ilić and Q. Liu, *Toward Sensing, Communications and Control Architectures for Frequency Regulation in Systems with Highly Variable Resources*. New York, NY: Springer New York, 2012, pp. 3–33.

[32] J. A. Mueller, M. Rasheduzzaman, and J. W. Kimball, "A model modification process for grid-connected inverters used in islanded microgrids," *IEEE Transactions on Energy Conversion*, vol. 31, no. 1, pp. 240–250, March 2016.

[33] V. Purba, S. V. Dhople, S. Jafarpour, F. Bullo, and B. B. Johnson, "Reduced-order structure-preserving model for parallel-connected three-phase grid-tied inverters," in *IEEE 18th Workshop on Control and Modeling for Power Electronics (COMPEL)*, 2017, pp. 1–7.

[34] M. L. Chan, R. Dunlop, and F. Schweppe, "Dynamic equivalents for average system frequency behavior following major distribances," *IEEE Transactions on Power Apparatus and Systems*, no. 4, pp. 1637–1642, 1972.
[35] P. M. Anderson and M. Mirheydar, "A low-order system frequency response model," *IEEE Transactions on Power Systems*, vol. 5, no. 3, pp. 720–729, 1990.
[36] H. Khalil, *Nonlinear Systems*, 3rd ed. Upper Saddle River, NJ: Prentice Hall, 2002.
[37] R. A. Horn and C. R. Johnson, *Matrix analysis*. Cambridge university press, 2012.
[38] A. Moeini and I. Kamwa, "Analytical concepts for reactive power based primary frequency control in power systems," *IEEE Transactions on Power Systems*, vol. 31, no. 6, pp. 4217–4230, November 2016.
[39] S. Boyd and L. Vandenberghe, *Convex Optimization*. Cambridge University Press, 2004.
[40] D. Liberzon, *Calculus of variations and optimal control theory: A concise introduction*. Princeton University Press, 2012.
[41] N. Li, C. Zhao, and L. Chen, "Connecting automatic generation control and economic dispatch from an optimization view," *IEEE Transactions on Control of Network Systems*, vol. 3, no. 3, pp. 254–264, Sept 2016.
[42] M. Parvania and R. Khatami, "Continuous-time marginal pricing of electricity," *IEEE Transactions on Power Systems*, vol. 32, no. 3, pp. 1960–1969, May 2017.
[43] T. Athay, R. Podmore, and S. Virmani, "A practical method for the direct analysis of transient stability," *IEEE Transactions on Power Apparatus and Systems*, no. 2, pp. 573–584, 1979.
[44] M. A. Pai, *Energy function analysis for power system stability*. Springer Science & Business Media, 2012.
[45] J. Chow and G. Rogers, *Power System Toolbox*. Cherry Tree Scientific Software, 2000.
[46] (2016) IEEE Power and Energy Society distribution test feeders. [Online]. Available: https://ewh.ieee.org/soc/pes/dsacom/testfeeders/.

Swaroop S. Guggilam (S'15) received the Bachelor's degree in electrical engineering from the Veermata Jijabai Technological Institute, Mumbai, Maharashtra, India, in 2013 and M.S. degree in electrical engineering from the University of Minnesota, Minneapolis, MN, USA, in 2015. He is currently working toward the Ph.D. degree in electrical engineering from the University of Minnesota, Minneapolis, MN, USA.

His research interests include distribution networks, optimization, power system modeling, analysis and control for increasing renewable integration.

Changhong Zhao (S'12-M'15) received the B. Eng. degree in Automation from Tsinghua University in 2010, and the PhD degree in Electrical Engineering from California Institute of Technology in 2016. His PhD thesis won the Caltech Demetriades-Tsafka-Kokkalis Prize and the Caltech Charles Wilts Prize. He is currently a Research Engineer with National Renewable Energy Laboratory, Golden, CO, USA, with research interests in power system dynamics and stability, optimal power flow, distributed control of smart grid, and multi-energy systems.

Emiliano Dall'Anese (S'08-M'11) received the Laurea Triennale (B.Sc Degree) and the Laurea Specialistica (M.Sc Degree) in Telecommunications Engineering from the University of Padova, Italy, in 2005 and 2007, respectively, and the Ph.D. In Information Engineering from the Department of Information Engineering, University of Padova, Italy, in 2011. From January 2009 to September 2010, he was a visiting scholar at the Department of Electrical and Computer Engineering, University of Minnesota, USA. From January 2011 to November 2014 he was a Postdoctoral Associate at the Department of Electrical and Computer Engineering and Digital Technology Center of the University of Minnesota, USA. Since December 2014 he has been a Senior Engineer at the National Renewable Energy Laboratory, Golden, CO, USA.

His research interests lie in the areas of Optimization Theory and Signal Processing. Current applications pertain to distributed optimization and control of large-scale complex energy systems and power-grid analytics.

Yu Christine Chen (S'10–M'15) received the B.A.Sc. degree in engineering science from the University of Toronto, Toronto, ON, Canada, in 2009, and the M.S. and Ph.D. degrees in electrical engineering from the University of Illinois at Urbana-Champaign, Urbana, IL, USA, in 2011 and 2014, respectively.

She is currently an Assistant Professor with the Department of Electrical and Computer Engineering, The University of British Columbia, Vancouver, BC, Canada, where she is affiliated with the Electric Power and Energy Systems Group. Her research interests include power system analysis, monitoring, and control.

Sairaj V. Dhople (S'09-M'13) received the B.S., M.S., and Ph.D. degrees in electrical engineering, in 2007, 2009, and 2012, respectively, from the University of Illinois, Urbana-Champaign. He is currently an Assistant Professor in the Department of Electrical and Computer Engineering at the University of Minnesota (Minneapolis), where he is affiliated with the Power and Energy Systems research group. His research interests include modeling, analysis, and control of power electronics and power systems with a focus on renewable integration. Dr. Dhople received the National Science Foundation CAREER Award in 2015. He currently serves as an Associate Editor for the IEEE Transactions on Energy Conversion.